ACS APPLIED MATERIALS & INTERFACES

Research Article

www.acsami.org

Bias-Polarity Dependent Ultraviolet/Visible Switchable Light-Emitting Devices

Pei-Nan Ni,[†,‡] Chong-Xin Shan,*[,†] Bing-Hui Li,[†] Shuang-Peng Wang,[†] and De-Zhen Shen*[,†]

[†]State Key Laboratory of Luminescence and Applications, Changchun Institute of Optics, Fine Mechanics and Physics, Chinese Academy of Sciences, Changchun 130033, China

[‡]University of Chinese Academy of Sciences, Beijing 100049, China

ABSTRACT: By taking semiconductors with different band-gap energies as the active layers and controlling the electron−hole recombination region through the electric field, bias-polarity dependent ultraviolet/visible switchable light-emitting devices have been realized in Au/MgO/$Mg_{0.49}Zn_{0.51}O$/$Mg_xZn_{1-x}O$/*n*-ZnO structures, of which the emission bands can be switched from the ultraviolet region to the orange region by changing the polarity of the applied bias. The results reported here may provide a feasible idea to multicolor-switchable light-emitting devices.

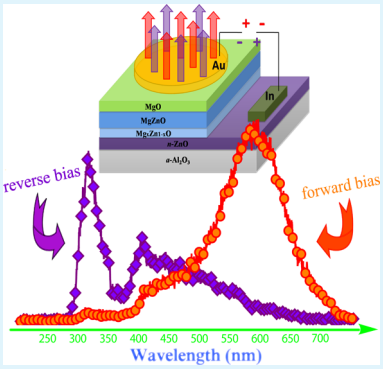

KEYWORDS: *ultraviolet, light-emitting devices, wide-band-gap semiconductors, color-switchable, accelerated electrons, magnesium zinc oxide*

1. INTRODUCTION

Semiconductor-based solid-state light sources, e.g., light-emitting devices (LEDs), have profoundly changed the way humans generate light for general lighting applications.[1−3] At present, a remarkably broad range of spectral bands, from near-infrared to deep ultraviolet, have been covered by this kind of light source.[4−6] A semiconductor-based light source featuring low power consumption, high efficiency, compact size, long lifetime, etc., is believed to be an ideal light source and benefit humanity at large.[7−10] Moreover, continuing efforts have been paid to this area to improve the performance of the solid-state light sources in keeping with a variety of practical requirements. It is well-known that semiconductors are characterized by a band-gap energy (E_g), which determines the energy of the photon produced when an electron in the conduction band recombines with a hole in the valence band, i.e., $h\nu = E_g$. The above fact means that the emission spectral band of a LED will be fixed once the active layer of the device is chosen. However, multicolor-switchable light-emitting devices, of which the emission band can be changed by varying the bias, are of great importance for multicolored flat panel displays, indicators, back-lights, etc.[11,12] Although many commercial approaches have been proposed, such as using a planar arrangement of red, green, and blue (RGB) color filters to subtractively create saturated RGB colors from white light,[13,14] and integrating side-by-side single-color RGB devices that produce additive multicolored emissions,[15] such multicolored devices are always problematic due to the unavoidable energy loss caused by the filters or the high cost and complexity resulting from the integration. In view of practical use, multicolor-switchable devices should utilize a relatively simple structure, of which the color can be switched by the magnitude of applied voltage or by the polarity of the applied bias. To this end, lots of color-switchable devices with relatively simple structures, including organic light-emitting diodes and inorganic thin-film electroluminescent devices, have been proposed and demonstrated in visible bands.[11,16−18] Meanwhile, it will be of great importance to further extend the spectral region of these kinds of color-switchable devices, such as to the ultraviolet region and to the infrared region.[19] However, no report on a UV/visible switchable device can be found up to date.

MgZnO alloy is a promising candidate for ultraviolet optoelectronic devices due to the wide variation of band-gap energy (3.37−7.8 eV).[20,21] Moreover, MgZnO alloys have many unique characters, such as the relatively low growth temperatures (100−750 °C), the high resistance to radiation, the environmentally friendly characteristics, etc.,[22−26] which make it an ideal choice as the ultraviolet light emitter under the excitation of accelerated electrons.

In this paper, semiconductor-based color-switchable LEDs have been fabricated from Au/$Mg_{0.49}Zn_{0.51}O$/$Mg_xZn_{1-x}O$/*n*-ZnO structures, of which the emission bands can be switched from the ultraviolet region to the orange region by changing the polarity of the applied bias. The emission mechanism has been

Received: February 19, 2014
Accepted: May 8, 2014
Published: May 8, 2014

   dx.doi.org/10.1021/am5010283 | *ACS Appl. Mater. Interfaces* 2014, 6, 8257−8262

discussed in terms of the carrier transportation process under the drive of applied bias.

2. EXPERIMENTAL DETAILS

The fabrication processes of the devices are detailed as follows: Firstly, a 570 nm ZnO layer with an electron concentration of 2.5×10^{18} cm^{-3} and a Hall mobility of 66 cm^2 V^{-1} s^{-1} was used as the conducting layer in this structure. The *n*-ZnO conducting layer was deposited on an *a*-plane sapphire substrate using a VG V80H plasma-assisted molecular-beam epitaxy (MBE). The detailed growth conditions can be found elsewhere.[27] A 200 nm $Mg_xZn_{1-x}O$ composition-gradient layer with a Mg content changing gradually from 0 to 0.49 was deposited onto the *n*-ZnO conducting layer via the MBE. Our previous work has demonstrated that the $Mg_xZn_{1-x}O$ composition-gradient layer can help to prevent the occurrence of phase separation in the MgZnO layer deposited onto it.[28] In order to fabricate the $Mg_xZn_{1-x}O$ composition-gradient layer, the Mg content was adjusted by increasing the temperature of the Mg cell from 310 to 340 °C at a rate of 0.02 °C/s gradually, while the temperature of the ZnO cell was fixed at 280 °C. The O_2 gas was activated in an Oxford Applied Research plasma cell (Model HD25) with a radio frequency operating at 13.56 MHz at a fixed power of 300 W. During the growth process, the substrate temperature was kept at 500 °C and the chamber pressure at 5.2×10^{-6} Torr. After that, a 380 nm $Mg_{0.49}Zn_{0.51}O$ active layer was deposited onto the $Mg_xZn_{1-x}O$ composition-gradient layer. A 100 nm MgO layer was used as the electron-accelerating layer due to its dielectric properties, which was deposited onto the $Mg_{0.49}Zn_{0.51}O$ active layer in a reactive radio-frequency magnetron sputtering technique using a 99.99% magnesium target in a mixed gas of oxygen and argon with a flow ratio of 1:2 at 400 °C. Finally, a semitransparent Au layer was deposited onto the MgO layer and an In layer onto the ZnO layer in vacuum evaporation, respectively, acting as electrodes.

A Hall measurement system (LakeShore 7707) was used to evaluate the electrical properties of these films. The absorption spectra of the layers were recorded using a Shimadzu UV-3101PC spectrophotometer. The Mg content in the MgZnO layer was determined by energy-dispersive X-ray spectroscopy. Photoluminescence (PL) spectra of the layers were measured by employing either a He–Ag laser (λ = 224 nm) or a He–Cd laser (λ = 325 nm) as the excitation sources. The current–voltage (*I*–*V*) characteristics of the structures were measured using a Keithley 2611A System, and the emission spectra were recorded in a Hitachi F4500 spectrometer at room temperature with a continuous-current power source.

3. RESULTS AND DISCUSSION

The inset of Figure 1 shows the schematic diagram and emissions recording geometry of the Au/MgO/$Mg_{0.49}Zn_{0.51}O$/$Mg_xZn_{1-x}O$/*n*-ZnO structure. As indicated in the figure, this structure shows a weak rectification behavior at both forward and reverse bias regions, where the reverse bias is defined as the situation where the Au electrode is biased negatively. To evaluate the optical band-gap energy of the MgZnO active layer, the absorption spectra of the MgZnO films have been measured, as shown in Figure 2a. The absorption component of the $Mg_xZn_{1-x}O$ composition-gradient layer can be recognized by comparing the absorption spectra of the MgZnO films both with and without the $Mg_xZn_{1-x}O$ layer, as indicated by an arrow. The band-gap energy of the $Mg_{0.49}Zn_{0.51}O$ layer deduced from the plot of $(ah\nu)^2$ vs $h\nu$ (a and $h\nu$ are the absorption coefficient and photon energy, respectively) is around 4.16 eV, as indicated in the inset of Figure 2a. Furthermore, the Mg content of the $Mg_xZn_{1-x}O$ layer is proved to almost linearly increase along the growth direction according to its content distribution, as shown in Figure 2b.

Figure 3a shows the emission spectra of the structure under different reverse biases. Under the reverse bias of −25 V, two

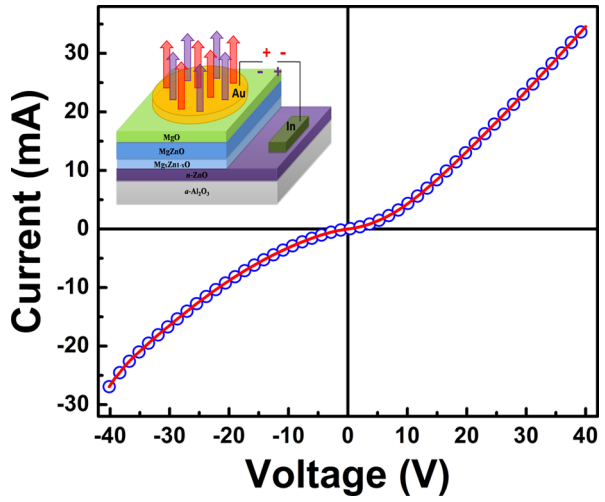

Figure 1. Current–voltage characteristics of the Au/MgO/$Mg_{0.49}Zn_{0.51}O$/$Mg_xZn_{1-x}O$/*n*-ZnO structure, and the inset shows the schematic diagram and emissions recording geometry of the structure.

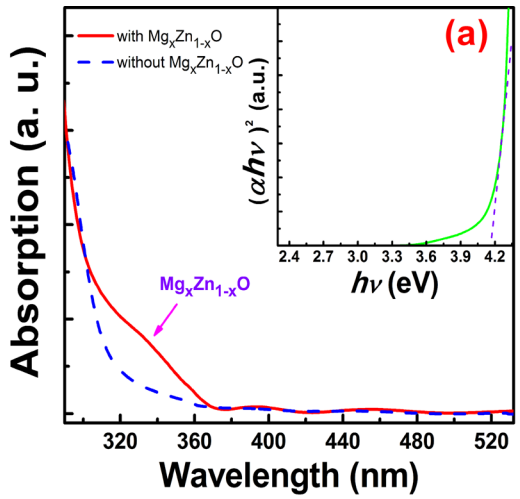

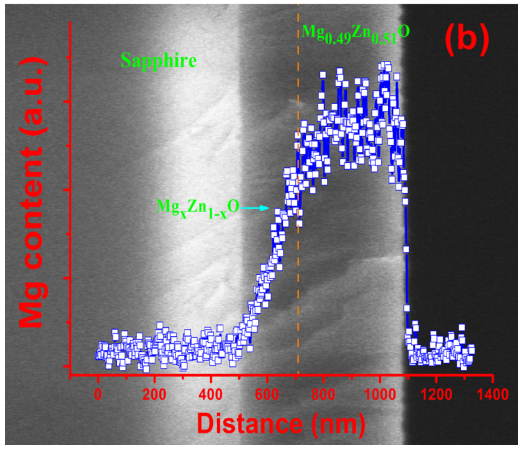

Figure 2. (a) Absorption spectra of the MgZnO films both with and without the $Mg_xZn_{1-x}O$ layer, and the inset shows a plot of $(ah\nu)^2$ vs $h\nu$. (b) The SEM image of the MgZnO films with a $Mg_xZn_{1-x}O$ layer; the inset shows the line profile of the Mg content.

emission bands located at around 310 and 400 nm, can be observed. Since the emissions at around 310 nm (4.00 eV) are close to the band-gap energy of the $Mg_{0.49}Zn_{0.51}O$ derived from

dx.doi.org/10.1021/am5010283 | ACS Appl. Mater. Interfaces 2014, 6, 8257–8262

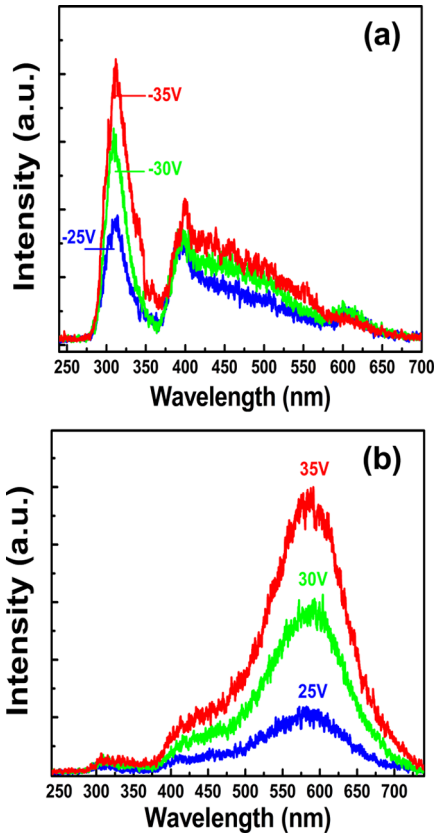

Figure 3. Emission spectra of the Au/MgO/$Mg_{0.49}Zn_{0.51}O$/$Mg_xZn_{1-x}O$/*n*-ZnO structure under reverse bias conditions (a) and forward bias conditions (b).

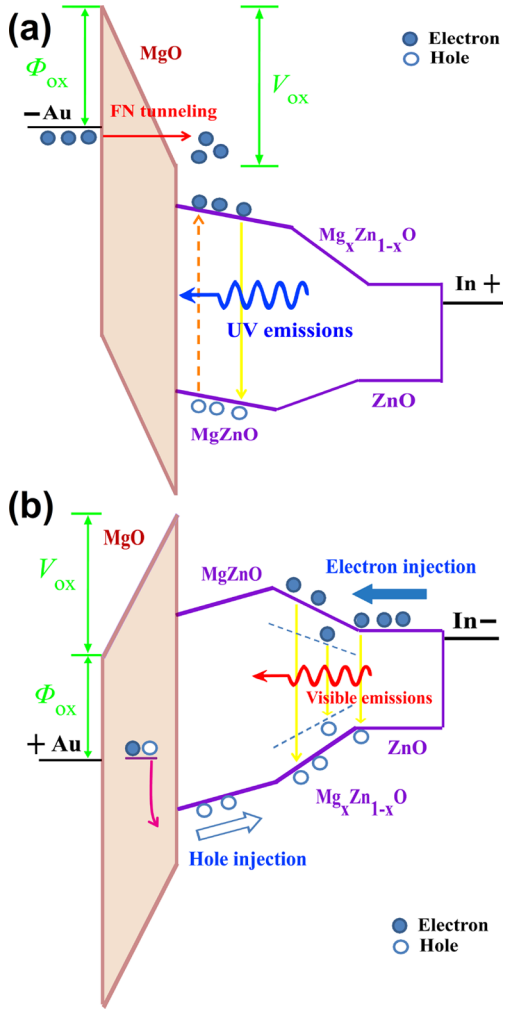

Figure 4. Band diagrams of the Au/MgO/$Mg_{0.49}Zn_{0.51}O$/$Mg_xZn_{1-x}O$/*n*-ZnO structure under reverse bias conditions (a) and forward bias conditions (b).

the absorption spectra (4.16 eV), it can be attributed to the near-band-edge (NBE) emissions of the $Mg_{0.49}Zn_{0.51}O$ layer. Note that this emission increases significantly with further increasing the bias, as evidenced in Figure 3a. More interestingly, the dominant emission band of this structure can be switched after changing the polarity of the applied bias, as shown in Figure 3b. It can be seen that the structure shows strong emissions at around 590 nm, and a weak emission band extending from 300 to 360 nm in the ultraviolet region can also be detected. As the applied bias increased, the emissions at around 590 nm increased dramatically, whereas the ultraviolet emissions hardly changed. Furthermore, an emission band at about 405 nm that may come from the *n*-ZnO layer can be recognized at higher forward bias.

The mechanism of the above emissions from this structure under both reverse and forward biases can be understood in terms of the band alignment of the structure, as shown in Figure 4: Under reverse bias, such as at −25 V bias, due to the dielectric nature of MgO, most of the bias voltage would be applied onto this layer so that the voltage drop across the MgO layer (V_{ox}) is much larger than the barrier height for the electrons (Φ_{ox} = 4.3 eV). Under this condition, the effective width of the triangular Schottky potential barrier for the electrons will be reduced significantly; thus, many electrons can tunnel through the MgO layer via the Fowler−Nordheim (FN) tunneling.[29] Considering that the thickness of the MgO layer is only about 100 nm, the electric field in the MgO will be very high; e.g., it will be as high as 2.5×10^6 V/cm at −25 V bias. Thus, when the electrons coming from the Au electrode enter into this layer, they will be accelerated greatly and gain much kinetic energy by the high electric field in this layer. Once these accelerated electrons gain enough energy and enter into the $Mg_{0.49}Zn_{0.51}O$ active layer, they will excite the electrons in the valence band of the $Mg_{0.49}Zn_{0.51}O$ layer into its conduction band. In this way, electron−hole pairs will be generated in this layer under the excitation of the accelerated electrons.[28,30] Then, the free electrons may recombine radiatively with the generated holes. As a result, UV emission from the $Mg_{0.49}Zn_{0.51}O$ active layer will be detected, as shown in Figure 3a. Note that a broad emission band at about 400 nm can also be found under reverse bias; it may come from the *n*-ZnO layer or the $Mg_xZn_{1-x}O$ layer due to the absorption of the UV emissions from the $Mg_{0.49}Zn_{0.51}O$ layer. Since only the region of the $Mg_{0.49}Zn_{0.51}O$ layer within the depth of penetration of the accelerated electrons will be excited, the light-emitting area under the excitation of accelerated electrons is confined to the region in the $Mg_{0.49}Zn_{0.51}O$ layer close to the interface between the MgO layer and the $Mg_{0.49}Zn_{0.51}O$ layer. In the case of forwards bias, likewise, the electrons in the conduction bands of the $Mg_{0.49}Zn_{0.51}O$ layer, although few in number, will tunnel into the MgO layer. Then, these tunneling electrons as well as the carriers in the MgO layer will gain much kinetic energy due to the high electric field in this layer and initiate the impact ionization process, giving rise to free electrons and holes, which

dx.doi.org/10.1021/am5010283 | ACS Appl. Mater. Interfaces 2014, 6, 8257−8262

has been elucidated in our previous publications.[31,32] After that, the generated holes will be drifted to the $Mg_{0.49}Zn_{0.51}O$ layer by the electric field. Since the resistivity of the $Mg_{0.49}Zn_{0.51}O$ layer is too large to be measured by our Hall system, one can speculate that there are few electrons in the conduction band of the $Mg_{0.49}Zn_{0.51}O$ layer. As a result, the holes can travel quite a long distance in this layer before they recombine with electrons. Meanwhile, electrons in the conduction band of the *n*-ZnO layer will move toward the positive electrode under the drive of the electric field. Because of the barrier effect of the $Mg_xZn_{1-x}O$ for the electrons, most of the electrons will accumulate in the conduction band of the $Mg_xZn_{1-x}O$ layer, as depicted in Figure 4b. Then, when the holes move into this region, they will recombine with these accumulated electrons. However, probably because of the large lattice and thermal expansion coefficient mismatches within this layer, there are so many deep-level centers that the deep-level related emissions, namely, the orange emissions, are more prominent than either the NBE emission of the $Mg_xZn_{1-x}O$ or the *n*-ZnO, as shown in Figure 3b.

To further confirm the origin of the orange emission under forward bias condition, the PL characteristics of the MgO/$Mg_{0.49}Zn_{0.51}O$/$Mg_xZn_{1-x}O$/*n*-ZnO structure under the excitation of a 224 nm laser from the MgO side have been measured, as shown in Figure 5a. It can be seen that a strong emission

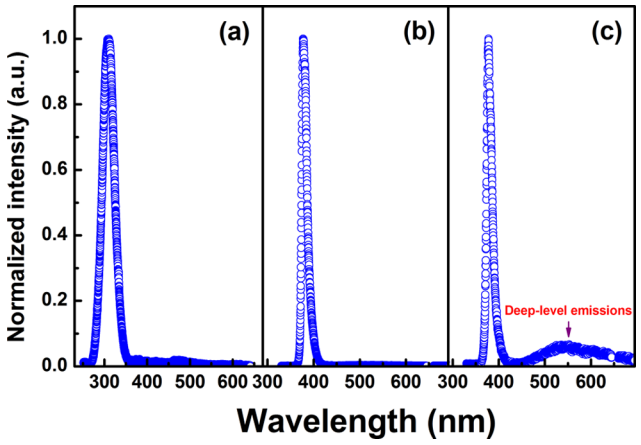

Figure 5. (a) PL spectra of the Au/MgO/$Mg_{0.49}Zn_{0.51}O$/$Mg_xZn_{1-x}O$/*n*-ZnO structure excited by a 224 nm laser. (b) PL spectra of the *n*-ZnO conducting layer excited by a 325 nm laser. (c) PL spectra of the Au/MgO/$Mg_{0.49}Zn_{0.51}O$/$Mg_xZn_{1-x}O$/*n*-ZnO structure excited by a 325 nm laser.

band at about 309 nm dominates the spectrum, whereas no obvious deep-level related emission or NBE emission of ZnO can be detected, which proves the good optical quality of the $Mg_{0.49}Zn_{0.51}O$ layer. The emissions at around 309 nm, which are almost identical to those shown in Figure 3a, can be attributed to the NBE emissions of the $Mg_{0.49}Zn_{0.51}O$ layer. Since the 224 nm laser can only penetrate into a thin region of the $Mg_{0.49}Zn_{0.51}O$ layer due to the strong absorption, similar to the case under the reverse bias, both the $Mg_xZn_{1-x}O$ layer and the *n*-ZnO conducting layer will not be excited in this condition. Meanwhile, the *n*-ZnO conducting layer used in this structure is proved to have good optical quality without any defect-related emissions under the excitation of a 325 nm laser, as shown in Figure 5b. Considering that the absorption of the $Mg_{0.49}Zn_{0.51}O$ layer at 325 nm is weak, as shown in Figure 2a, a 325 nm laser was used to excite the MgO/$Mg_{0.49}Zn_{0.51}O$/$Mg_xZn_{1-x}O$/*n*-ZnO structure from the MgO side, as shown in Figure 5c. In this condition, both the $Mg_xZn_{1-x}O$ layer and the *n*-ZnO conducting layer will be excited, and obvious deep-level related emissions can be observed from the MgO/$Mg_{0.49}Zn_{0.51}O$/$Mg_xZn_{1-x}O$/*n*-ZnO structure, besides the NBE emissions of the *n*-ZnO conducting layer. On the basis of the above experimental results, one can deduce that the orange emissions shown in Figure 3b come from the deep-level related emissions of the $Mg_xZn_{1-x}O$ layer.

Figure 6 shows the emission intensity−voltage characteristics of the structure at UV regions and orange regions, respectively.

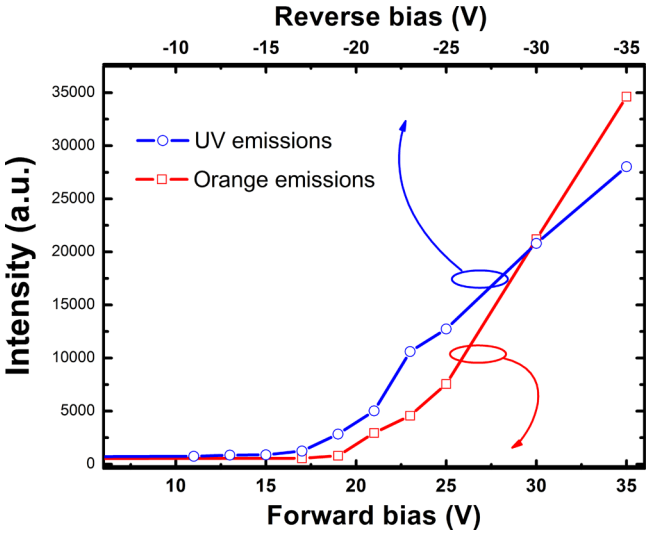

Figure 6. Intensity−voltage characteristics of the Au/MgO/$Mg_{0.49}Zn_{0.51}O$/$Mg_xZn_{1-x}O$/*n*-ZnO structure under both forward and reverse bias conditions.

The UV emissions increase superlinearly with the applied voltage under reverse bias conditions. Likewise, the orange emissions increase with the bias voltage under forward bias conditions. Moreover, the turn-on voltage of the UV emissions (about 17 V) is smaller than that of the orange emissions (about 21 V), which can also be understood in terms of the band alignment of the structure shown in Figure 4. Considering that most of the bias voltage will be applied onto the MgO layer, the bias voltage determines the magnitude of the electric field in this layer, which, in turn, determines the energy that the carriers will gain through the acceleration process. Meanwhile, according to the work of Anderson,[33] in a direct-band-gap semiconductor with spherical constant energy surfaces and constant effective masses m_c^* and $m_v^* = \gamma m_c^*$ for electrons in the conduction and valence bands, respectively, the threshold energy for a phononless ionization process initiated by an electron can be expressed by the following formula

$$E_{th} = E_g\left(\frac{2+\gamma}{1+\gamma}\right) \quad (1)$$

where E_g is the band-gap energy, and m_c^* and m_v^* are taken at the bottom of the conduction band and the top of the valence band, and γ is the ratio between m_c^* and m_v^*. Therefore, the threshold voltage increases with the band-gap energy. In other words, less kinetic energy will be required for the accelerated carriers to generate electron−hole pairs in the $Mg_{0.49}Zn_{0.51}O$ layer compared with the case in the MgO layer via the impact

ionization process. Consequently, the UV emissions have a lower turn-on voltage than the orange emissions.

4. CONCLUSION

In conclusion, color-switchable LEDs have been realized in a Au/MgO/$Mg_{0.49}Zn_{0.51}O$/$Mg_xZn_{1-x}O$/*n*-ZnO structure. The emission bands of this structure can be switched from the ultraviolet region to the orange region by changing the polarity of the applied bias. The results reported in this paper demonstrated that, by controlling the recombination region of the excess carriers through the electric fields, bias-polarity-dependent multicolor-switchable light-emitting devices can be realized. Furthermore, in this structure, the excess carriers for the UV emissions are generated under the excitation of accelerated electrons, and the excess holes for the visible emissions are generated through the impact ionization process. The above mechanisms can lead to light emissions from semiconductors by bypassing the doping issues, which is known to be more difficult as the band-gap energy increases. Therefore, the above ideas can also be applied to other semiconductor materials to realize color-switchable devices.

AUTHOR INFORMATION

Corresponding Authors

*E-mail: shancx@ciomp.ac.cn.

*E-mail: shendz@ciomp.ac.cn .

Notes

The authors declare no competing financial interest.

ACKNOWLEDGMENTS

This work is supported by the National Basic Research Program of China (2011CB302005), the Natural Science Foundation of China (11074248, 11134009, 10974197, 11374296, and 61177040), and the Science and Technology Developing Project of Jilin Province (20111801).

REFERENCES

(1) Schubert, E. F.; Kim, J. K. Solid-State Light Sources Getting Smart. *Science* **2005**, *308*, 1274−1278.

(2) Tsukazaki, A.; Ohtomo, A.; Onuma, T.; Ohtani, M.; Makino, T.; Sumiya, M.; Ohtani, K.; Chichibu, S. F.; Fuke, S.; Segawa, Y.; Ohno, H.; Koinuma, H.; Kawasaki, M. Repeated Temperature Modulation Epitaxy for P-Type Doping and Light-Emitting Diode Based on ZnO. *Nat. Mater.* **2005**, *4*, 42−46.

(3) Waltereit, P.; Brandt, O.; Trampert, A.; Grahn, H. T.; Menniger, J.; Ramsteiner, M.; Reiche, M.; Ploog, K. H. Nitride Semiconductors Free of Electrostatic Fields for Efficient White Light-Emitting Diodes. *Nature* **2000**, *406*, 865−868.

(4) Taniyasu, Y.; Kasu, M.; Makimoto, T. An Aluminum Nitride Light-Emitting Diode with a Wavelength of 210 Nanometres. *Nature* **2006**, *441*, 325−328.

(5) Shen, H.; Wang, S.; Wang, H.; Niu, J.; Qian, L.; Yang, Y.; Titov, A.; Hyvonen, J.; Zheng, Y.; Li, L. S. Highly Efficient Blue-Green Quantum Dot Light-Emitting Diodes Using Stable Low-Cadmium Quaternary-Alloy ZnCdSSe/ZnS Core/Shell Nanocrystals. *ACS Appl. Mater. Interfaces* **2013**, *5*, 4260−4265.

(6) Tessler, N.; Medvedev, V.; Kazes, M.; Kan, S.; Banin, U. Efficient Near-Infrared Polymer Nanocrystal Light-Emitting Diodes. *Science* **2002**, *295*, 1506−1508.

(7) Oh, J. H.; Yang, S. J.; Do, Y. R. Healthy, Natural, Efficient and Tunable Lighting: Four-Package White LEDs for Optimizing the Circadian Effect, Color Quality and Vision Performance. *Light: Sci. Appl.* **2014**, *3*, e141.

(8) Ra, Y. H.; Navamathavan, R.; Park, J. H.; Lee, C. R. High-Quality Uniaxial $In_xGa_{1-x}N$/GaN Multiple Quantum Well (MQW) Nanowires (NWs) on Si(111) Grown by Metal-Organic Chemical Vapor Deposition (MOCVD) and Light-Emitting Diode (LED) Fabrication. *ACS Appl. Mater. Interfaces* **2013**, *5*, 2111−2117.

(9) Nakamura, S. The Roles of Structural Imperfections in InGaN-Based Blue Light-Emitting Diodes and Laser Diodes. *Science* **1998**, *281*, 956−961.

(10) Oh, J. H.; Yang, S. j.; Sung, Y. G.; Do, Y. R. Improved Color Coordinates of Green Monochromatic pc-LED Capped with a Band-Pass Filter. *Opt. Express* **2013**, *21*, 4539−4550.

(11) Heikenfeld, J.; Steckl, A. J. Rare-Earth-Doped GaN Switchable Color Electroluminescent Devices. *IEEE Trans. Electron Devices* **2002**, *49*, 1545−1551.

(12) Poelma, R. H.; Tarashioon, S.; van Zeijl, H. W.; Goldbach, S.; Ziji, J. L. J.; Zhang, G. Q. Multi-LED package design, fabrication and thermal analysis. *J. Semicond.* **2013**, *34*, 054002.

(13) Kido, J.; Kimura, M.; Nagai, K. Multilayer White Light-Emitting Organic Electroluminescent Device. *Science* **1995**, *267*, 1332−1334.

(14) Sabnis, R. W. Color Filter Technology for Liquid Crystal Displays. *Display* **1999**, *20*, 119−129.

(15) Wu, C. C.; Sturm, J. C.; Register, R. A.; Thompson, M. E. Integrated Three Color Organic Light Emitting Devices. *Appl. Phys. Lett.* **1996**, *69*, 3117−3119.

(16) Hong, Y. J.; Lee, C. H.; Yoon, A.; Kim, M.; Seong, H. K.; Chung, H. J.; Sone, C.; Park, Y. J.; Yi, G. C. Visible-Color-Tunable Light-Emitting Diodes. *Adv. Mater.* **2011**, *23*, 3284−3288.

(17) Nakamura, K.; Ishikawa, T.; Nishioka, D.; Ushikubo, T.; Kobayashia, N. Color-Tunable Multilayer Organic Light Emitting Diode Composed of DNA Complex and Tris(8-hydroxyquinolinato)-aluminum. *Appl. Phys. Lett.* **2010**, *97*, 193301.

(18) Mori, T.; Obata, K.; Imaizumi, K.; Mizutani, T. Preparation and Properties of an Organic Light Emitting Diode with Two Emission Colors Dependent on the Voltage Polarity. *Appl. Phys. Lett.* **1996**, *69*, 3309−3311.

(19) Hajialamdari, M.; Strickland, D. Tunable Mid-Infrared Source from an Ultrafast Two-Color Yb:Fiber Chirped-Pulse Amplifier. *Opt. Lett.* **2012**, *37*, 3570−3572.

(20) Hou, Y. N.; Mei, Z. X.; Liu, Z. L.; Zhang, T. C.; Du, X. L. $Mg_{0.55}Zn_{0.45}O$ Solar-Blind Ultraviolet Detector with High Photoresponse Performance and Large Internal Gain. *Appl. Phys. Lett.* **2011**, *98*, 103506.

(21) Tanaka, H.; Fujita, S.; Fujita, S. Fabrication of Wide-Band-Gap $Mg_xZn_{1-x}O$ Quasi-ternary Alloys by Molecular-Beam Epitaxy. *Appl. Phys. Lett.* **2005**, *86*, 192911.

(22) Zhao, Y. M.; Zhang, J. Y.; Jiang, D. Y.; Shan, C. X.; Zhang, Z. Z.; Yao, B.; Zhao, D. X.; Shen, D. Z. Ultraviolet Photodetector Based on a MgZnO Film Grown by Radio-Frequency Magnetron Sputtering. *ACS Appl. Mater. Interfaces* **2009**, *1*, 2428−2430.

(23) Choopun, S.; Vispute, R. D.; Yang, W.; Sharma, R. P.; Venkatesan, T.; Shen, H. Realization of Band Gap above 5.0 eV in Metastable Cubic-Phase $Mg_xZn_{1-x}O$ Alloy Films. *Appl. Phys. Lett.* **2002**, *80*, 1529.

(24) Auret, F. D.; Goodman, S. A.; Hayes, M.; Legodi, M. J.; van Laarhoven, H. A.; Look, D. C. Electrical Characterization of 1.8 MeV Proton-Bombarded ZnO. *Appl. Phys. Lett.* **2001**, *79*, 3074.

(25) Etacheri, V.; Roshan, R.; Kumar, V. Mg-Doped ZnO Nanoparticles for Efficient Sunlight-Driven Photocatalysis. *ACS Appl. Mater. Interfaces* **2012**, *4*, 2712−2725.

(26) Chen, N. B.; Sui, C. H. Recent Progress in Research on $Mg_xZn_{1-x}O$ Alloys. *Mater. Sci. Eng., B* **2006**, *126*, 16−21.

(27) Ni, P. N.; Shan, C. X.; Wang, S. P.; Li, B. H.; Zhang, Z. Z.; Zhao, D. X.; L, L.; Shen, D. Z. Enhanced Responsivity of Highly Spectrum-Selective Ultraviolet Photodetectors. *J. Phys. Chem. C* **2012**, *116*, 1350−1353.

(28) Ni, P. N.; Shan, C. X.; Li, B. H.; Shen, D. Z. High Mg-Content Wurtzite MgZnO Alloys and Their Application in Deep-Ultraviolet Light-Emitters Pumped by Accelerated Electrons. *Appl. Phys. Lett.* **2014**, *104*, 032107.

(29) Sze, S. M. *Physics of Semiconductor Devices*, 2nd ed.; John Wiley and Sons: New York, 1981.

(30) Ni, P. N.; Shan, C. X.; Wang, S. P.; Li, B.H.; Zhang, Z. Z.; Shen, D. Z. Ultraviolet Emissions Excited by Accelerated Electrons. *Opt. Lett.* **2012**, *37*, 1568−1570.
(31) Zhu, H.; Shan, C. X.; Zhang, J. Y.; Zhang, Z. Z.; Li, B. H.; Zhao, D. X.; Yao, B.; Shen, D. Z.; Fan, X. W.; Tang, Z. K.; Hou, X.; Choy, K. L. Low-Threshold Electrically Pumped Random Lasers. *Adv. Mater.* **2010**, *22*, 1877−1881.
(32) Zhu, H.; Shan, C. X.; Li, B. H.; Zhang, Z. Z.; Yao, B.; Shen, D. Z. Deep-Ultraviolet Light-Emitting Device Realized via a Hole-Multiplication Process. *Appl. Phys. Lett.* **2011**, *99*, 101110.
(33) Anderson, C. L.; Crowell, C. R. Threshold Energies for Electron-Hole Pair Production by Impact Ionization in Semiconductors. *Phys. Rev. B* **1972**, *5*, 2267−2272.